TITLE

GLIDER AND SATELLITE HIGH RESOLUTION MONITORING OF A MESOSCALE EDDY IN THE ALGERIAN BASIN: EFFECTS ON THE MIXED LAYER DEPTH AND BIOCHEMISTRY

AUTHORS

Yuri Cotroneo, Università degli Studi di Napoli “Parthenope”, Naples, Italy.

Giuseppe Aulicino, Università degli Studi di Napoli “Parthenope”, Naples, Italy.

Simón Ruiz, Instituto Mediterráneo de Estudios Avanzados, IMEDEA(CSIC-UIB), Esporles, Spain.

Ananda Pascual, Instituto Mediterráneo de Estudios Avanzados, IMEDEA(CSIC-UIB), Esporles, Spain.

Giorgio Budillon, Università degli Studi di Napoli “Parthenope”, Naples, Italy and Consorzio Interuniversitario Nazionale per la Fisica delle Atmosfere e delle Idrosfere, CINFAI, Tolentino (MC), Italy.

Giannetta Fusco, Università degli Studi di Napoli “Parthenope”, Naples, Italy and Consorzio Interuniversitario Nazionale per la Fisica delle Atmosfere e delle Idrosfere, CINFAI, Tolentino (MC), Italy.

Joaquin Tintoré, Balearic Islands Coastal Observing and Forecasting System (SOCIB), Palma de Mallorca, Spain and Instituto Mediterráneo de Estudios Avanzados, IMEDEA(CSIC-UIB), Esporles, Spain

CORRESPONDING AUTHOR: YURI COTRONEO yuri.cotroneo@uniparthenope.it

ABSTRACT

Despite an extensive bibliography for the circulation of the Mediterranean Sea and its sub-basins, the debate on mesoscale dynamics and their impacts on bio-chemical processes is still open because of their intrinsic time scales and of the difficulties in their sampling. In order to clarify some of these processes, the “Algerian BAsin Circulation Unmanned Survey - ABACUS” project was proposed and realized through access to the JERICO Trans National Access (TNA) infrastructure between September and December 2014. In this framework, a deep glider cruise was carried out in the area between the Balearic Islands and the Algerian coast to establish a repeat line for monitoring of the basin circulation. During the mission a mesoscale eddy, identified on satellite altimetry maps, was sampled at high-spatial horizontal resolution (4 km) along its main axes and from the surface to 1000 m depth. Data were collected by a Slocum glider equipped with a pumped CTD and biochemical sensors that collected about 100 complete casts inside the eddy. In order to describe the structure of the eddy, in situ data were merged with next generation remotely sensed data: daily synoptic sea surface temperature (SST) and chlorophyll concentration (Chl-a) images from the MODIS satellites, as well as sea surface height and geostrophic velocities from AVISO. From its origin along the Algerian coast in the eastern part of the basin, the eddy propagated northwest at a mean speed of about 4 km/day, with a mean diameter of 112-130 km, mean amplitude of 15.7 cm; the eddy was clearly distinguished from the surrounding waters thanks to its higher SST and Chl-a values. Temperature and salinity values over the water column confirm the origin of the eddy from the Algerian Current (AC) showing the presence of recent Atlantic water in the surface layer and Levantine Intermediate Water (LIW) in the deeper layer. The eddy footprint is clearly evident in the multiparametric vertical sections conducted along its main axis.

Deepening of temperature, salinity and density isolines at the center of the eddy is associated with variations in Chl-a, oxygen concentration and turbidity patterns. In particular, at 50 m depth along the eddy borders, Chl-a values are higher (1.1-5.2 μg/l) in comparison with the eddy center (0.5-0.7 μg/l) with maximum values found in the southeastern sector of the eddy.

Calculation of geostrophic velocities along transects and vertical quasi-geostrophic velocities (QG-w) over a regular 5 km grid from the glider data helped to describe the mechanisms and functioning of the eddy. QG-w presents an asymmetric pattern, with relatively strong downwelling in the western part of the eddy and upwelling in the southeastern part. This asymmetry in the vertical velocity pattern, which brings LIW into the euphotic layer as well as advection from the northeastern sector of the eddy, may explain the observed increases in Chl-a values.

1 INTRODUCTION

The Algerian Basin occupies most of the southern part of the Western Mediterranean Sea and is characterized by the presence of both fresh surface waters coming from the Atlantic (Atlantic Water - AW) and more saline waters from the Mediterranean region (Millot, 1999, 2006). The interaction between AW and the resident saltier waters occurs at different scales, including the basin-scale, sub-basin–scale and mesoscale structures that together characterize the basin dynamics (Robinson and Golnaraghi 1994; Fusco et al., 2003; Vidal-Vijande et al. 2011).

AW flows along the Algerian slope, forming the Algerian Current (AC), the along-slope flow that drives this water mass from Gibraltar to the rest of the Western and Eastern Mediterranean basins (Millot, 1985). Due to complex hydrodynamical processes, this along-slope current generally becomes unstable, meanders and generates mesoscale eddies (e.g., Millot, 1985; Font et al., 1998; Font et al. 2004; Salas et al. 2002; Olita et al., 2011). A typical AC instability can be described as a meander associated with cyclonic and anticyclonic mesoscale eddies (Moran et al., 2001). Previous studies based on in-situ and satellite data have described the typical origins, paths and evolution of these structures (Millot, 1999; Ruiz et al., 2002; Taupier-Letage et al., 2003; Millot and Taupier-Letage, 2005). According to these studies, AC meanders usually carry an embedded (coastal) anticyclonic eddy that is associated with an upwelling cell on its southwestern side; often there is an accompanying short-lived shallow cyclonic circulation on the meander crest (e.g., Obaton et al., 2000; Moran et al., 2001).

The anticyclonic eddies (hereafter Algerian Eddies, AEs) can rapidly grow to up to 50–100 km in diameter, reach vertical extents of hundreds or thousands of meters (Ruiz et al., 2002), and drift eastwards along the slope at a few km/day. Owing to topographic forcing when approaching the Sardinia channel, they successively separate from the AC and drift northward. AEs then skirt the Sardinian slope where they interact with the Levantine Intermediate Water (LIW) vein (Millot, 1987; Millot and Taupier-Letage, 2005). Finally, AEs propagate offshore (westward) into the central part of the basin, following a counterclockwise pathway in the Eastern Algerian Basin that can also include several loops (Millot, 1999; Fuda et al., 2000; Ruiz et al., 2002; Taupier-Letage et al., 2003).

AEs have been observed since the 1980s in satellite infrared images (Taupier-Letage and Millot, 1988), and can last for many months or even years (Millot et al., 1997; Puillat et al., 2002). They can have a strong impact on the general circulation of the entire Algerian Basin, with marked repercussions for the distribution of water masses and biochemical parameters and, hence, on ecosystems. For example, when located along the Algerian slope AEs can dramatically alter the AC, eventually forcing the latter to flow perpendicularly to the coast for months (Millot et al., 1997;

Taupier-Letage and Millot, 1988), altering its usual along slope flow (Font et al., 1998). More recent studies using satellite altimetry data and numerical modelling (Pujol and Larnicol, 2005; Pascual et al., 2007 and 2014; Escudier, 2015) have shown that the AC and associated eddies are characterized by high levels of eddy kinetic energy.

Studies based on remote sensing have shown close correlation between thermal and ocean color satellite signatures, demonstrating that mesoscale dynamics modulate biological activity (Arnone and La Violette, 1986; Taupier-Letage, 1988; Arnone et al., 1990; Taupier-Letage et al., 2003). Consequently, biological activity is also characterized by large mesoscale spatial and temporal variability (e.g., Lohrenz et al., 1988a, 1988b; Robinson, 1983; Morel and André, 1991). A large anticorrelation between sea level anomalies and phytoplankton biomass has also been found by Olita et al., (2011) in the central zone of the basin, suggesting a clear biological response to the shoaling/deepening of isopycnals, and thus to nutrient injection (removal) into (out of) the euphotic layer.

To describe these processes it is therefore important to conduct frequent multi-platform and mesoscale-dedicated monitoring activities in the study area with data collection at small sampling intervals, without neglecting useful information from larger spatial scales. To properly address these scientific challenges, new technologies for in situ data collection, mainly Autonomous Underwater Vehicles (AUVs) and reliable satellite data are being progressively implemented. AUVs allow the collection of high resolution physical and biological data, providing useful contributions to the understanding of mesoscale and sub-mesoscale dynamics (Ruiz et al., 2009) while remote sensing provides a better understanding of the processes at basin scale.

This paper focuses on the description of the structure of a mesoscale eddy in space and depth and its effects on mixed layer depth and biochemistry. In this work we take advantage of new technologies combining use of AUV observations and a large set of satellite-observed variables. In particular, a Slocum deep glider mission was carried out during September-December 2014 in the framework of the ABACUS (Algerian BAsin Circulation Unmanned Survey) project supported by the Joint European Research Infrastructure network for Coastal Observatories (JERICO).

The paper is structured as follows: first a description of the glider characteristics and mission, the satellite datasets and the methodology for the analysis performed on the data are presented; then the main results and discussion follow.

2 DATA AND METHODS

From September 15 to December 19 2014 two deep SLOCUM G2 glider missions were carried out in the Algerian Basin in the framework of the ABACUS project. The glider missions were supported by JERICO TransNational Access (TNA – Seventh framework programme) and were designed to perform a Mallorca-Algeria monitoring repeat line, and eventually investigate the presence of mesoscale structures thanks to the gliders' adaptive sampling capabilities. As a large surface eddy was detected in AVISO altimetry maps south east of Mallorca, the original sampling strategy for the first glider mission was modified. After concluding a first transect from Mallorca to Algeria, the glider sampling route was modified in order to cross the eddy along two transects collecting physical and biochemical measurements (Figure 1).

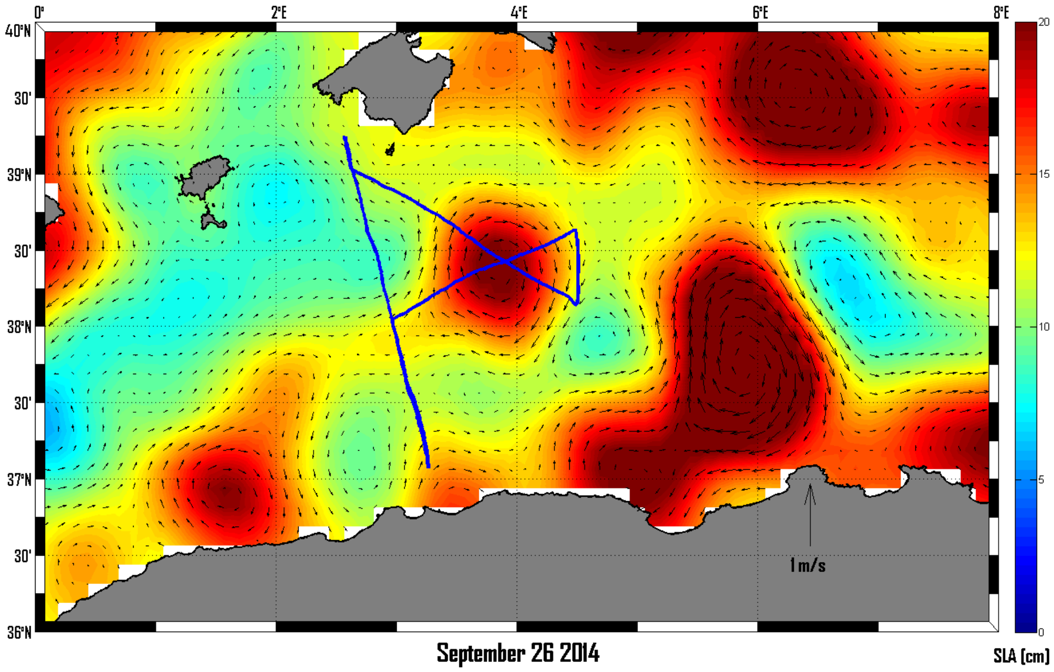

Figure 1: Sea level anomaly map (color scale) and associated geostrophic velocity anomalies (black arrows) from AVISO data on 26 September 2014. Blue line shows the glider track from 15 September to 20 October 2014.

In situ data collection was supported by continuous monitoring of remotely sensed data from different platforms. Successive satellite images of altimetry (AVISO), sea surface temperature (SST) and chlorophyll-a concentration (Chl-a) from NASA were used to depict the large scale dynamics of the area of interest for eddy presence, location of mesoscale structures and, consequently, definition of the sampling track.

2.1 GLIDER CHARACTERISTICS, SENSORS AND SAMPLING PLAN

Gliders are autonomous underwater vehicles providing high-resolution hydrographic and bio-chemical measurements. These vehicles control their buoyancy to allow vertical motion in the water column and make use of their hydrodynamic shape and small fins to make horizontal motions (Bouffard et al., 2010). In particular, ABACUS project field activities were performed in collaboration with the Balearic Islands Coastal Observing and Forecasting System (SOCIB) and Instituto Mediterráneo de Estudios Avanzados (IMEDEA CSIC-UIB) using a SLOCUM G2 glider for deep water (1000 m maximum depth) with a vertical speed of 0.18±0.02 m/s resulting in an horizontal velocity of about 0.36 m/s. Real time data transmission from the glider can be configured. For this mission this occurred every 8 km (6 hours) and permitted the retrieval of a first overview of the data collected, as well as transmission of new sampling and navigation directives to the glider.

In this paper we focus on the glider data from the mission conducted from 15 September to 20 October 2014 over the area of interest for the presence of a mesoscale eddy (Figure 1).

The pre-mission activities were carried out at the SOCIB glider facility (Tintoré et al., 2013) and included all ballasting and adjustment operations needed to assure the glider capability to reach the surface. Within this scope, the climatological maximum value of temperature and minimum value of salinity for the studied area and period have been analyzed. These data were used as extreme hydrographic characteristics of the water to be navigated and allowed us to derive the minimum density (1024.0683 Kg/m^3) needed to precisely tune the glider for the target waters.

Resolution of sampling was defined according to the scientific aims of the mission (high resolution in both horizontal and vertical directions) and considering the energetic constraints of the platform.

The data acquisition strategy was set in order to complete a saw-tooth navigation pattern (Figure 2) allowing the glider to dive with an angle of 26° between 20 and 975 m depth. The glider was programmed to sample only during downcasts (Figure 2 coloured lines) with a final alongtrack resolution of almost 4 km once the profile is normalized in the vertical. No data were collected during upcasts (Figure 2 black lines).

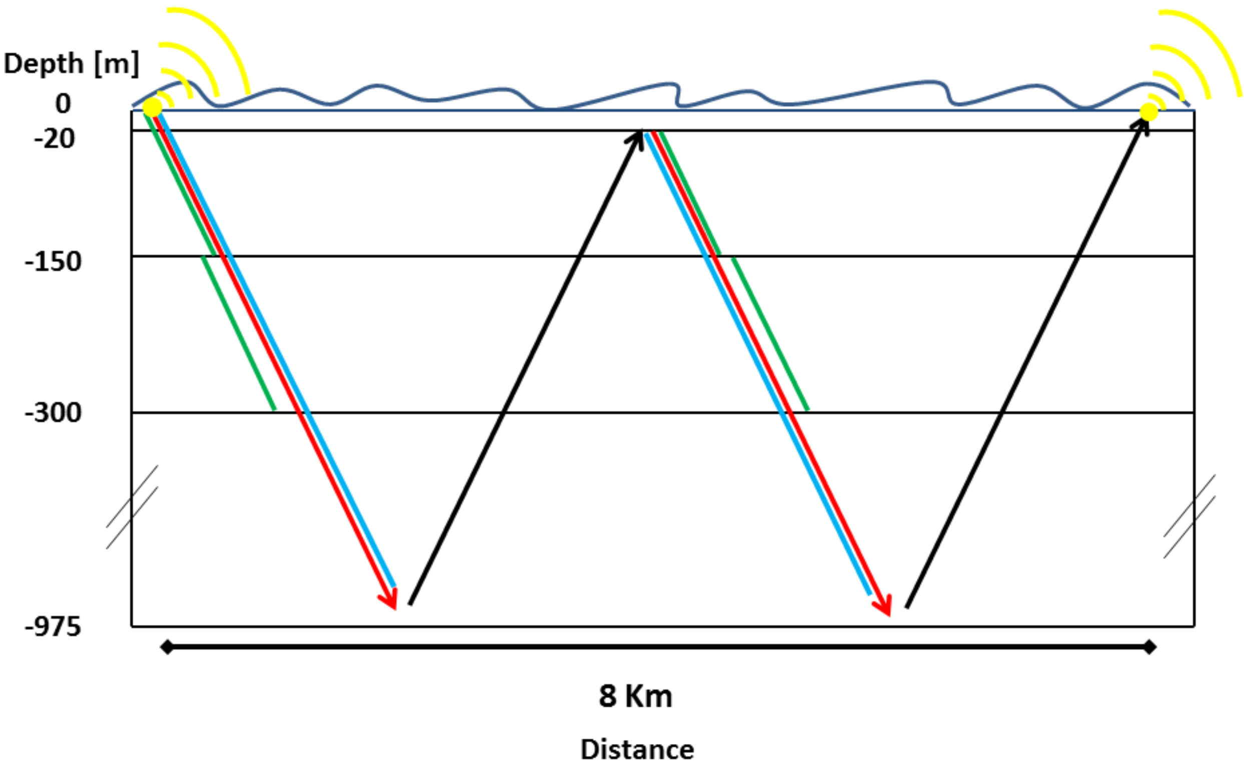

Figure 2: Slocum glider navigation and sampling scheme. During each downcast (red arrow) CTD and oxygen sensors (cyan line) sampled the water column from surface to 975 m, while optical parameters (green line) have been sampled down to 300 m with variable resolution (details in table 1). No data were acquired during upcasts (black arrows).

The glider platform carried a series of physical and biochemical sensors sampling the seawater at different rates according to depth as shown in table 1.

Parameter	Instrument	Sample rate (Hz)	Vertical resolution (m)	Depth range (m)
Temperature,Salinity, Depth	GPCTD - Glider payload pumped CTD by Seabird	1/2	0.4	-5/-1000
Oxygen	Optode 5013 by AADI	1/4	0.8	-5/-1000
Fluorescence, Turbidity	FLNTUslk by Wetlabs	1/8 1/16	1.6 3.2	-5/-150 -150/-300

Table1: Sampling rate and vertical resolution of glider data.

After the mission, data were transferred from the internal glider memory to the SOCIB Data Center where pre-processing, quality control and validation were carried out and production of level 1 and level 2 data occurred (Cusi et al., 2013) before the dissemination of the data on the web. In this paper, level 2 data of about 380 glider casts collected during the entire cruise were used.

Glider CTD profiles also allowed the calculation of surface geostrophic currents across the sections sampled by the glider. Aliasing linked to internal waves (Rundik and Cole, 2011) did not affect isobaric quantity since we focus the analysis on mesoscale structures (> 30 km). The reference level of 850 dbar was chosen as the maximum common depth for the sampled profiles and, on the basis of previous studies in the area, reporting velocities of about 1-2 cm/s at 800-1000 m (Millot, 2005), which is close to the level of no motion. Depth-averaged currents from glider data were not used due to possible large errors in the glider's compass, which introduces significant spurious velocities in the estimation of depth-averaged currents (Merckelbach et al. 2008).

2.2 ALTIMETRY DATA

Altimetry data over the entire Algerian Basin were used to investigate the main characteristics of the identified mesoscale eddy: its mean path, dimensions, sea surface elevation and translation speed.

In particular, multi-mission daily maps of Sea Level Anomaly (SLA), Geostrophic Velocity Anomalies, Absolute Dynamic Topography (ADT) and absolute geostrophic velocities from early June 2014 to November 2014 provided by AVISO-SSALTO/DUACS (http://www.aviso.altimetry.fr/en/data.html) system were used.

The entire dataset is available on a 1/8°x1/8° regular Cartesian grid over the Mediterranean Sea and results from the merging process of all altimeter missions (SARAL/AltiKa, Cryosat-2, HY2a, Jason-1&2, T/P, Envisat, GFO, ERS-1 & 2 and even Geosat). ADT data are computed by AVISO as the sum of SLA and mean dynamic topography (SMDT-MED-2014, Rio et al., 2014). In this work the "all sat merged" data series is used in order to guarantee a better quality of the data despite of the number of available satellites at a given time that may change over the period. In particular, from June to October 2014, data from four altimeter missions have been included in the selected dataset. Moreover the choice of the "all sat merged" dataset is also based on the fact that even if the horizontal resolution (1/8°) of SLA maps does not allow us to identify most of eddies with sizes smaller than thirty kilometres, Pascual et al. (2007) indicated that three altimeters are sufficient for a correct monitoring of the mesoscale circulation of the Mediterranean Sea and that four may resolve circulation features with sizes significantly smaller than 1/8° (Iacono et al., 2013). Furthermore Capet et al (2014) showed that the new AVISO dataset released in April 2014 offers an enhanced description of mesoscale activity, even within a 300 km coastal band, with more eddies detected and lower eddy radius estimates. Therefore, eddies with a radius of about 100 km, or slightly smaller, are expected to be sufficiently resolved over most of the dataset.

2.3 MODIS DATA

Sea Surface Temperature (SST) and Chlorophyll concentration (Chl-a) information acquired by NASA MODerate resolution Imaging Spectroradiometer (MODIS) Terra and Aqua satellites over the Western Mediterranean Sea have been included in this study. In particular, level-2 and level-3 Ocean Color (OC) and SST products acquired for the entire period of the glider mission (http://oceancolor.gsfc.nasa.gov) were used. The use of products at different processing levels depended on the specific investigation that was carried out. Level-3 at 4 km resolution averaged over 3-days were combined with altimetry information to perform a preliminary basin-scale analysis of the AC and to detect the presence and the evolution of mesoscale structures during September and October 2014. Level-2 daily data at 1 km resolution, instead, were used to study in detail the monitored eddy and to discuss its evolution during the glider cruise. The MODIS satellite constellation provided about twice daily diurnal imagery. Concerning SST, only night-time data were used in order to avoid any disturbance due to the insolation effect (Gentemann and Wentz, 2001). Furthermore, cloud cover effects were removed using a specific filter (Ackerman et al., 1997; Brown and Minnett, 1999). This operation reduced the amount of information in some scenes but considerably improved their quality and reliability. MODIS data have been processed, analyzed and visualized using Matlab and SEADAS, a comprehensive image analysis package for the processing, display, analysis, and quality control of ocean color data provided by NASA.

2.4 QUASI-GEOSTROPHIC THEORY

Vertical motion has been diagnosed using the quasi-geostrophic (QG) Omega equation, which is a well-known approach used in physical oceanography (Pinot et al., 1996). This indirect method can be applied in this case study since local the Rossby number is on the order of 0.1. To resolve the Omega equation, fields of geostrophic velocities and density are required along both space and depth. In this work, data are obtained from glider hydrographic measurements and some additional boundary conditions (w=0 for the upper and lower boundaries and Neumann conditions at the lateral boundaries).

The gridded fields of dynamic height and density used as inputs to solve the Omega equation, have been obtained through an Optimal Statistical Interpolation scheme (Gomis et al., 2001). Observations have been interpolated over a grid of 5 km resolution using a length scale correlation of 28 km derived empirically from observations. Moreover, small scales not resolved by the sampling have been filtered out using a low-pass filter (Pedder, 1993). In other words, only structures > 80 km diameter have been retained in the interpolated fields. This is a conservative approach but, given the distribution of the observations, it ensures that output fields are not contaminated by artificial structures from the interpolation process. The Optimal Statistical Interpolation scheme used is an algorithm that operates on 2D fields, so it is applied level by level from 20 to 850 m depth. Note that the interpolation has been performed in a reduced area where the observations properly resolve the scales considered in this analysis (> 80 km).

3 RESULTS

3.1 WATER MASSES

The θ/S diagram shows the presence of typical Mediterranean water masses (Figure 3). The surface layer (0-50 m) of most of the profiles is characterized by recent and old Atlantic Water (AW) presence while intermediate layers are occupied by Levantine Intermediate Water (LIW). As expected, the deepest layer shows the presence of a Western Mediterranean Deep Water (WMDW) signal.

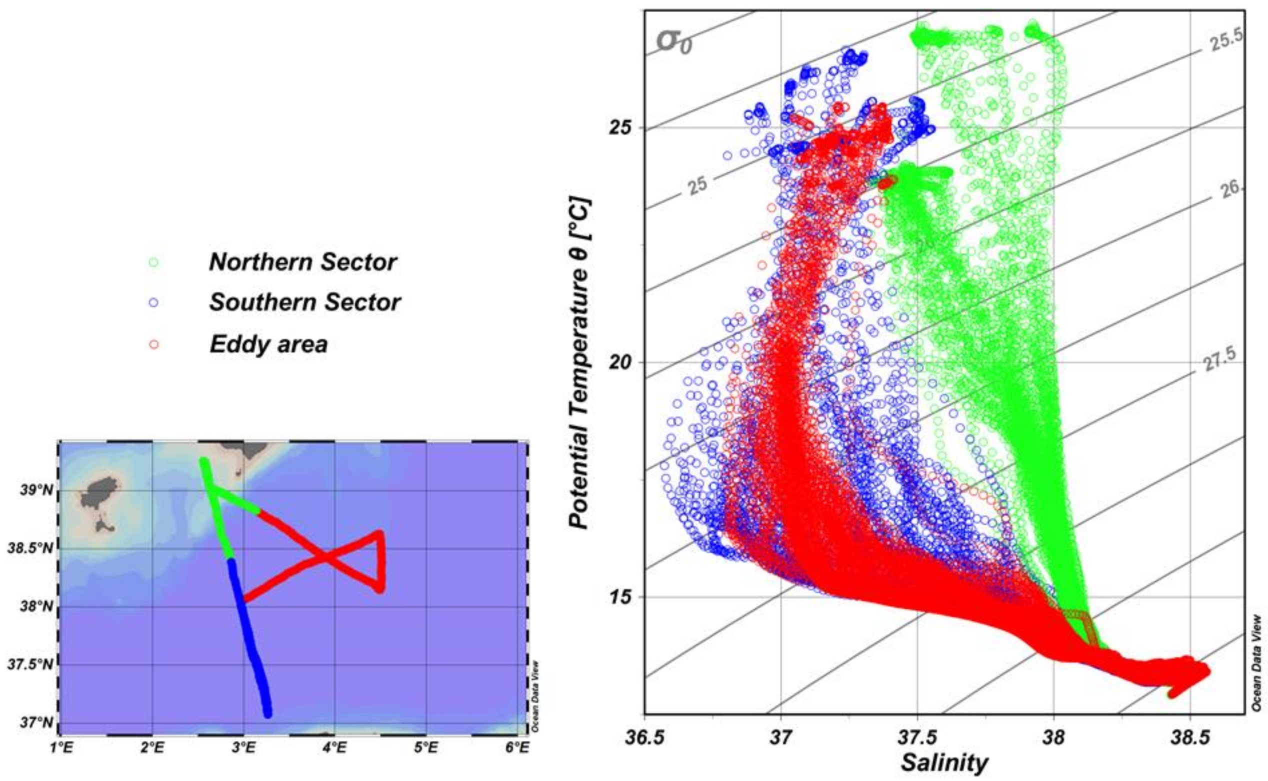

Figure 3: Potential temperature/salinity diagram (θ/S) for the entire glider mission. Blue and green circles identify data from the southern and northern sectors of the track respectively. Data associated with the eddy area are represented by red dots.

During this glider mission, AW properties are found to vary over a large range of values for both salinity (36.5-38.0) and temperature (15 °C-27.6 °C) according to different stages of mixing, geographical position and residence time in the Mediterranean Sea. Fresher and colder AW is found in the southern part of the basin, while more mixed and modified AW is found in the northern sectors of the glider path. In particular, northern sectors are characterized by the presence of the saltiest surface water identified during the mission, thanks to the high level of modification of the AW, as well as to the more Balearic characteristics of the water masses.

Below 300 m depth and beneath the AW layer, it is possible to identify the presence of LIW. Most profiles show the presence of LIW characterized by θ≤13.5° and S~38.5 and low oxygen concentration values. According to these thermohaline properties, the LIW identified during the glider mission may have followed the normal expected route, exiting from the Sardinia channel, flowing along the Western Sardinia slope and the French and Spanish slopes, and finally reaching the Algerian basin (Millot and Taupier-Letage, 2005).

WMDW is found in the deepest sampled layer between 800 and 1000 m depth, with typical θ values <13 °C and S values ranging between 38.43 and 38.46.

Similarity between water masses inside and outside the eddy structure can be clearly shown by dividing the entire mission into three legs. A northern leg (green dots) includes all the glider profiles sampled north of 38.4°N and of the eddy area, which are characterized by the presence of the saltier and more Balearic water at the surface as previously described, as well as by LIW presence at depth. The southern leg of the Mallorca-Algeria transect (blue dots) shows the expected presence of fresher water of recent Atlantic origin at the surface that is associated with the AC system and typical LIW presence from 300-600 m. Temperature and salinity values measured at the surface level inside the identified eddy (red dots) are more similar to water mass characteristics of the southern part of the basin (blue dots). The presence of recent AW water is clear and, again, the LIW core is identified at depths greater than 300 m. The correspondence of thermohaline properties of water masses inside the eddy with those identified in the southern part of the basin is a clear indication of the possible origin of the eddy from this area, and probably from a perturbation of the AC main flux. Moreover this hypothesis seems to perfectly agree with results derived from the satellite data analysis shown in section 3.5.

3.2 TEMPERATURE, SALINITY AND DENSITY SECTIONS

Potential temperature (θ), salinity (S) and potential density anomaly (σ_0) sections obtained through glider data along two transects crossing the eddy in the SW/NE and SE/NW directions are represented in figures 4 and 5 for the 0-800 m (a, b, c) and 0-150 m (d, e, f) layers. The data point to the presence of a strong seasonal thermocline at about 20/30 m. Above this thermocline, an area of higher salinity (37.34) centered at 3.75°W and temperature (25.4 °C at 3.5°W) is found in correspondence with the eddy center, while water masses with lower salinity (37.20) and temperature (24.6 °C) values occupy the surrounding area (Figures 4e, 4d, 5e, 5d). Below this surface layer, a typical anticyclonic thermohaline structure is seen with the expected deepening of isotherms in correspondence with the eddy center (13.5 °C at 250 m depth, figures 4a,5a). A stable salinity layer (S=37.00) reaches to 80 m depth in the center of the eddy and shallower depths (about 50 m) along its borders. In the 300-600 m layer, the salinity values rapidly increase due to the presence of LIW; about 38.50 with a core of more salty water (38.55/38.56) beneath the eddy center (Figures 4b, 5b). As expected and according to the anticyclonic circulation, the vertical extension of the LIW is larger in the center of the eddy than along its borders, as also described in previous studies focusing on anticyclonic eddies in the Algerian Basin (Ruiz et al., 2002).

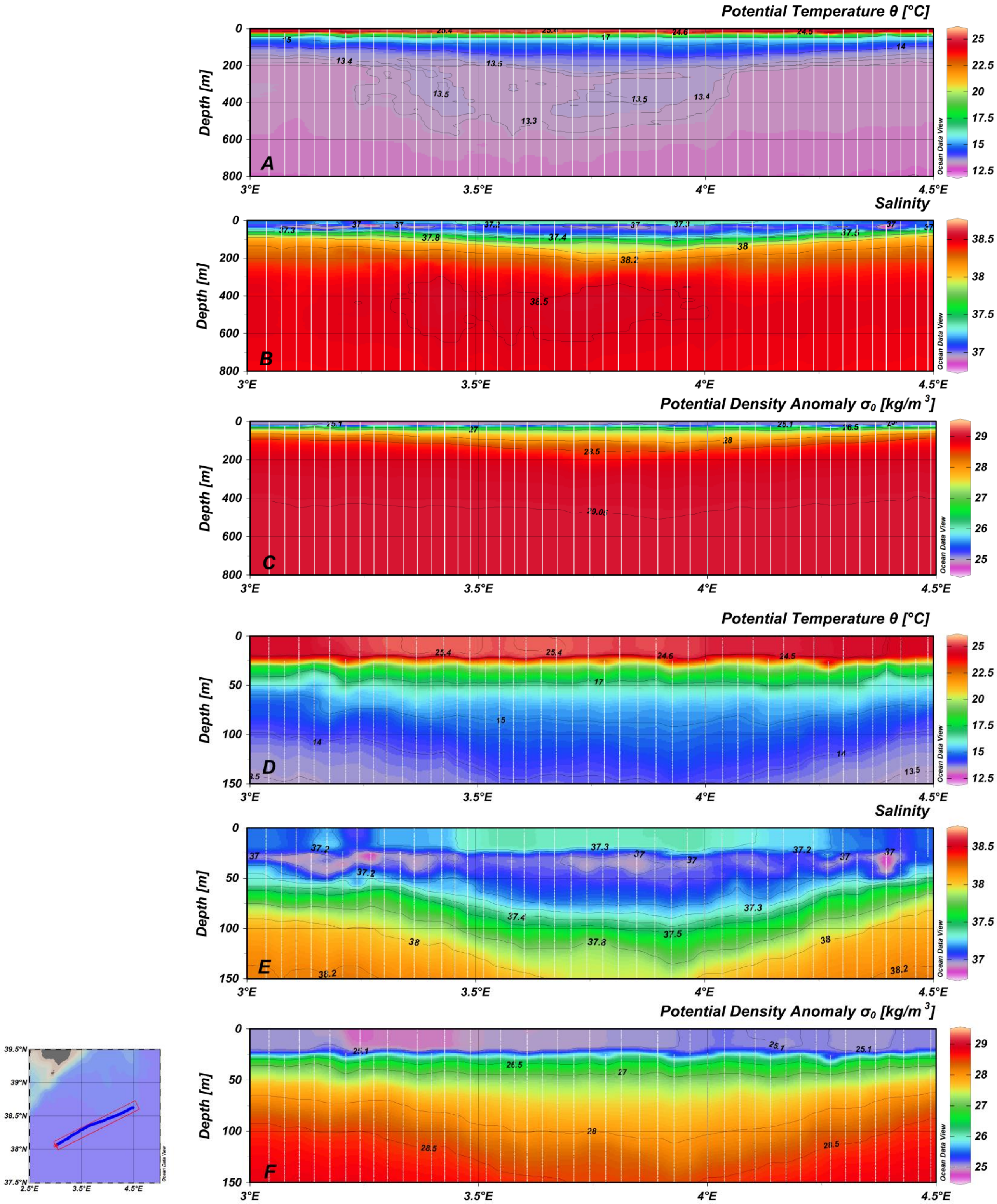

Figures 4: Sections from surface to 800 m depth of potential temperature θ (a), salinity (b) and potential density anomaly σ_0 (c) along the SW/NE axis of the eddy. The first 150 m of the water column for θ (d), salinity (e) and σ0 (f) are also shown.

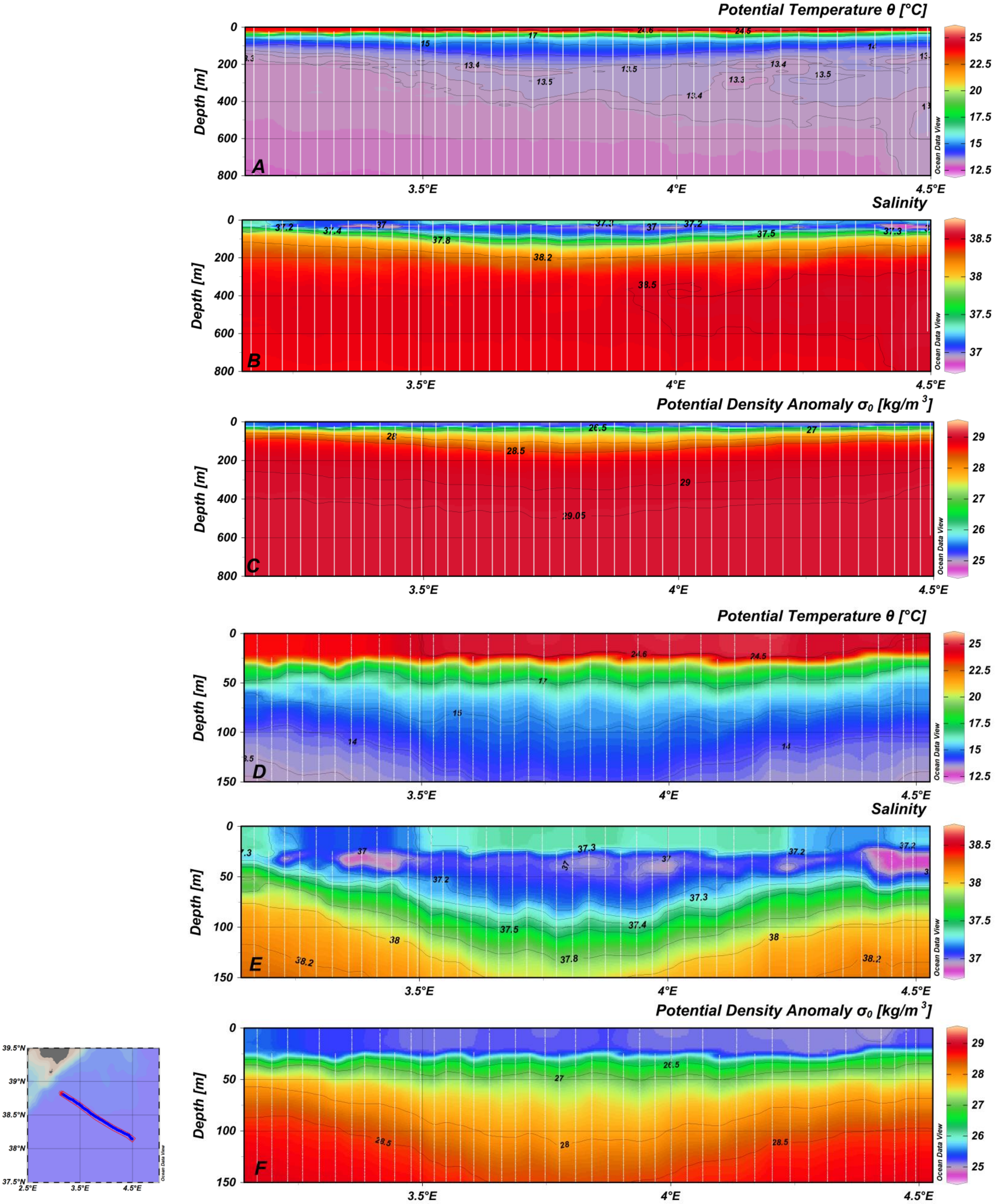

Figures 5: Sections from surface to 800 m depth of potential temperature θ (a), salinity (b) and potential density anomaly σ_0 (c) along the SE/NW axis of the eddy. The first 150 m of the water column for θ (d), salinity (e) and σ0 (f) are also shown.

In the 800-1000 m layer (not shown) the salinity decreases with depth due to the ending of the LIW signal, whose presence is confined within the 300-600 m layer. In correspondence with the eddy center, temperature data show the deepening of isolines at all sampled depth (Figures 4a, 5a).

Potential density anomaly sections from 0 to 800 m depth (Figures 4c, f and 5c, f) show the expected presence of a strong seasonal pycnocline and the deepening of isolines associated with the eddy circulation, with the 28.85 Kg/m^3 isoline reaching to about 300 m in correspondence with the eddy center.

The mixed layer depth (MLD) and maximum vertical extension of the eddy can be determined on the basis of θ, S and σ_0 profiles. The analysis of single glider casts show that the MLD is found to be located above a strong seasonal thermocline at about 20/25 m. The calculation of the MLD has also been tested against some objective criteria based on temperature and density profiles included in Kara et al. (2000), and confirm our estimates. During the entire glider cruise, σ_0 rapidly increases at the MLD from 25.1 kg/m^3 to 26.5 kg/m^3 and temperature decreases from more than 24.5 °C to about 17 °C (Figures 4d, e, f and 5d, e, f). The MLD does not seem to be affected by eddy presence, with profiles inside and outside the eddy showing the same water column structure. The maximum vertical extension reached by the eddy signal is ~300 m, where a clear deepening of potential temperature (13.48 °C), salinity (38.3) and density isolines (28.85 kg/m^3) is still evident in correspondence with the eddy center (Figures 4a, c and 5a, c).

This value is in agreement with previous studies (Ruiz et al., 2002; Isern-Fontanet et al., 2004) focusing on similar mesoscale structure in the study area.

3.3 OXYGEN AND CHLOROPHYLL CONCENTRATION SECTIONS

The glider biochemical instrumentation allowed us to sample oxygen, turbidity and chlorophyll content of water masses inside and outside the eddy. Optical measurements, including back-scattering and fluorescence, should be calibrated through in situ measurements and associated with the specific community composition (Cetinic et al., 2015). Nevertheless uncalibrated optical data collected during ABACUS mission can still be a useful proxy for the real concentration/abundance of the phytoplankton community.

As described in the data section, turbidity, Chl-a and O_2 parameter have been sampled at different rates with depth in order to better represent the surface and sub-surface layers along the SW/NE (Figures 6a, b, c) and SE/NW (Figures 7a, b, c) axes of the eddy.

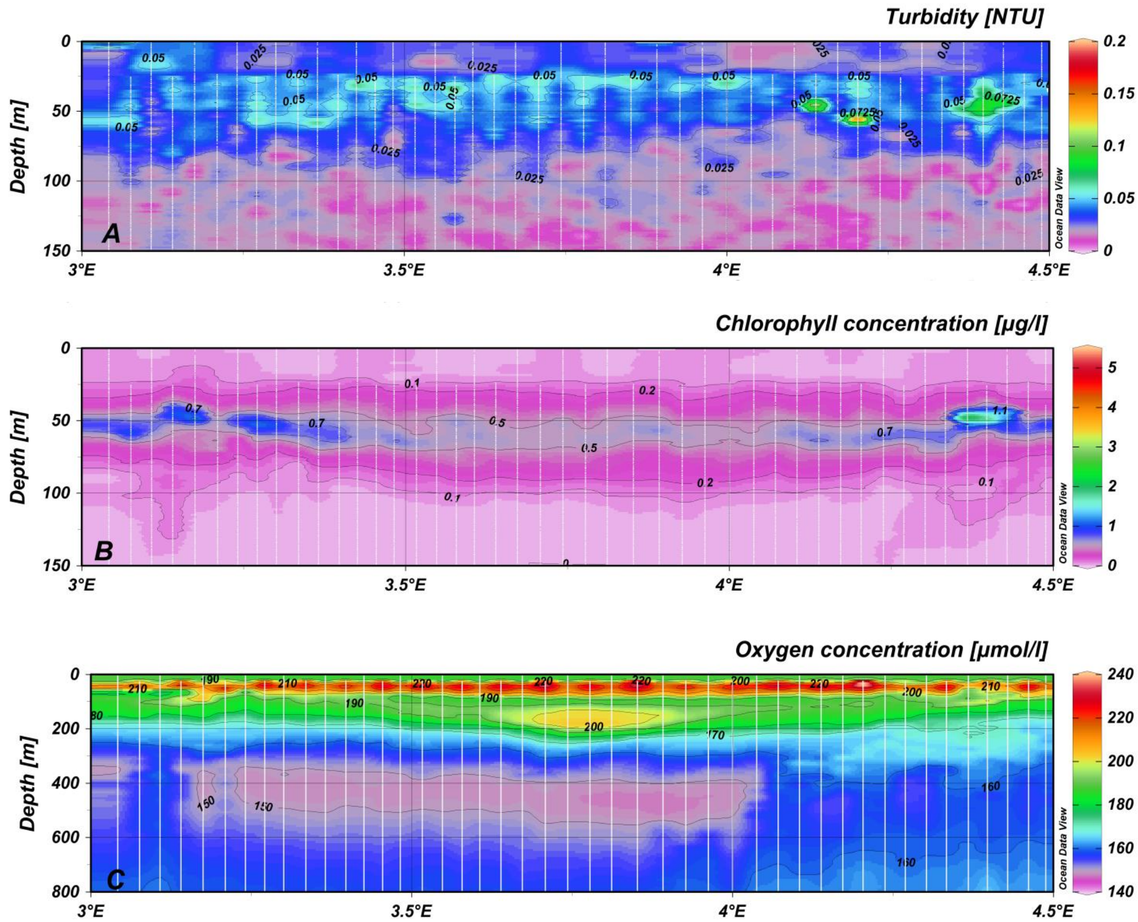

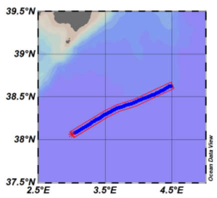

Figures 6: Sections from surface to 150 m depth of turbidity (a) and chlorophyll concentration (b) along the SW/NE axis of the eddy. Oxygen concentration (c) is shown for the 0-800 m layer.

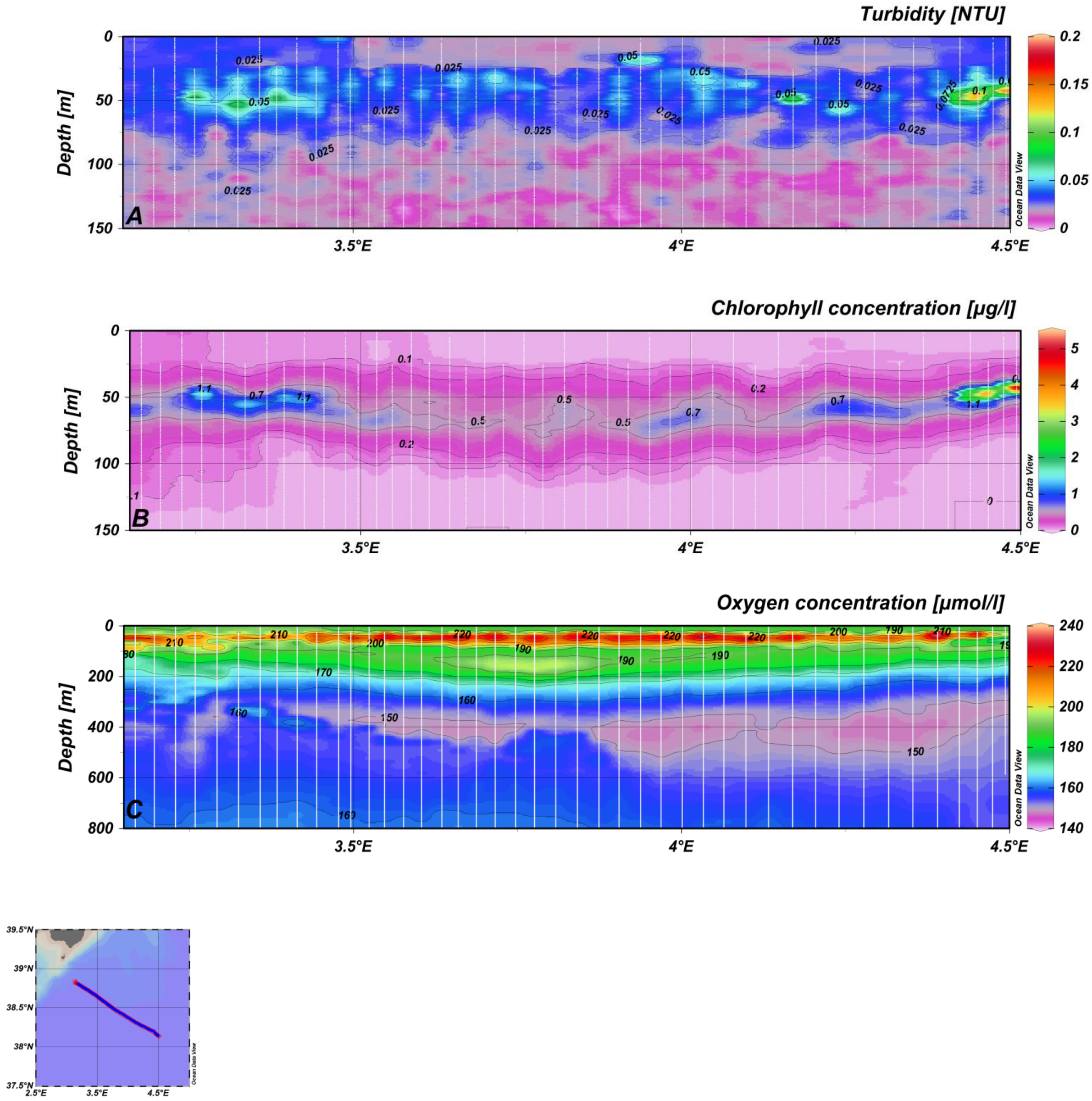

Figures 7: Sections from surface to 150 m depth of turbidity (a) and chlorophyll concentration (b) along the SE/NW axis of the eddy. Oxygen concentration (c) is shown for the 0-800 m layer.

Turbidity data (Figures 6a,7a) show the presence of the eddy footprint in the 0 – 70 m layer. In particular, increased signals (0.04/0.06 NTU) are found at about 50 m depth, with higher values (up to 0.15 NTU) in correspondence with eddy boundaries and the maximum turbidity value in the southeastern area of the eddy. The surface layer along both transects (depth < 20 m) is characterized by a positive NTU gradient from the centre of the eddy to its periphery, where shoaling of salinity and temperature isolines was noted while deeper layers (depth > 70 m) showed very low turbidity values along the transects.

During the entire cruise, turbidity data at about 20 m depth show the existence of marked differences between adjacent profiles. This difference may depend on variations in the vertical motion of the glider. In particular, data collected from profiles where the glider reaches the surface differ from data collected when the glider casts are limited to the 20-975 m layer. Nevertheless, the presence of high turbidity value at about 50 m as discussed above is not influenced by this anomalous behaviour.

A high sub-surface oxygen concentration layer (220 μmol/l) is found at about 50 m depth along all sections across the eddy (Figures 6c, 7c). As high differences between adjacent profiles are also found in the oxygen data relative to this layer, a further analysis will be required to reduce errors connected to glider vertical motion. Nevertheless, the presence of this high concentration layer is confirmed by measurements along all the transects. After a regular decrease, a relative maximum (200 μmol/l) is found just under the eddy center in both sections between 130 m and 200 m depth. This increase in oxygen concentration could be linked to the development of sub-mesoscale filaments in the mixed layer that may alternately upwell nutrients to the euphotic zone and downwell oxygen in the central part of the eddy (Niewiadomska et al., 2008; Perry et al., 2008; Brannigan et al., 2015).

Minimum values of 150 μmol/l are found between 400 m and 500 m depth and are associated with the presence of LIW (Figures 4b and 5b) in correspondence with the eddy center. After the end of the LIW signal, the O_2 concentration increases again to 160 μmol/l in the deepest sampled layer. Some asymmetry is present in the oxygen distribution in this layer; shoaling of the 160 μmol/l isoline is found, with the shallower (600 m) depth in the northeastern sector of the eddy, and the deeper layer (900-950 m) in the southwestern sector of the transect (depths >800 m not shown).

The chlorophyll distributions along the sections (Figures 6b, 7b) show relatively higher values (0.5/0.7 μg/l) at about 50 m depth along all the transects, while shallower and deeper layers are characterized by lower concentration values (< 0.2 μg/l). At 50 m depth the eddy footprint is clearly visible as an increase of Chl-a concentration along its borders. Along the SE/NW transect (Figure 7b), concentration values up to 5.2 μg/l are reached on the eastern border of the eddy, while a maximum concentration of 1.1 μg/l is found on its western side. The SW/NE section confirms the presence of higher values of Chl-a on the eddy borders and the relatively higher concentration on its eastern side (Figure 6b).

This distribution, with no significant chlorophyll concentration at surface and a sub-surface chlorophyll maximum at 50-100 m depth agrees with previous studies on eddy presence in the same area (Taupier-Letage et al, 2003), except for the presence of a relative Chl-a maximum at depth in correspondence with the eddy center that is not observed in the ABACUS mission dataset.

Taupier-Letage et al. (2003) also pointed out that an increase in Chl-a concentration was linked to the shoaling of isolines along the eddy borders and the possible contribution of Mediterranean waters (salinity>38) and associated nutrients to biological production. A similar distribution is shown from sections derived from glider data collected during the ABACUS mission. The shoaling of temperature, salinity and density isolines along the eddy borders characterizes a large layer including the depths where Chl-a maximum values are observed. This is also shown in figures 8a, b where Chl-a sections along the SW/NE (a) and SE/NW (b) transects are plotted together with the corresponding density values in order to highlight the correspondence between Chl-a maxima position and density variations.

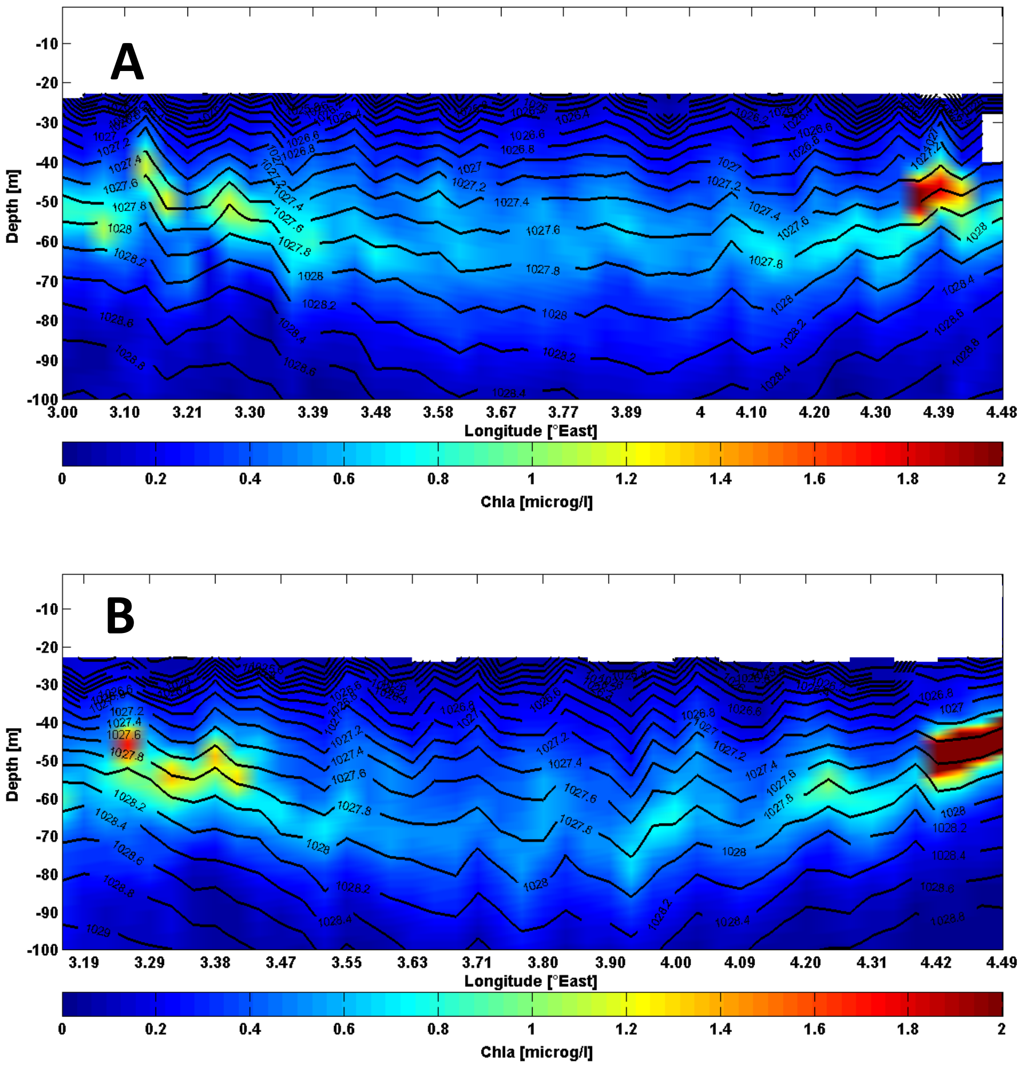

Figures 8: Sections from 20 m to 100 m depth of chlorophyll concentration (color scale) and potential density anomaly (black isolines) along the SW/NE (a) and SE/NW (b) axes of the eddy.

The horizontal asymmetry in Chl-a distribution between the eastern and western borders is well represented in figure 9. The horizontal map of Chl-a concentration at 45 m depth from glider data shows the highest values in the southeastern part of the eddy, with relatively higher values in the northeastern part of it. An increase in Chl-a concentration is found all along the eddy borders (indicated by the grey area) estimated from the minimum and maximum extent of the eddy on the basis of in situ and satellite data

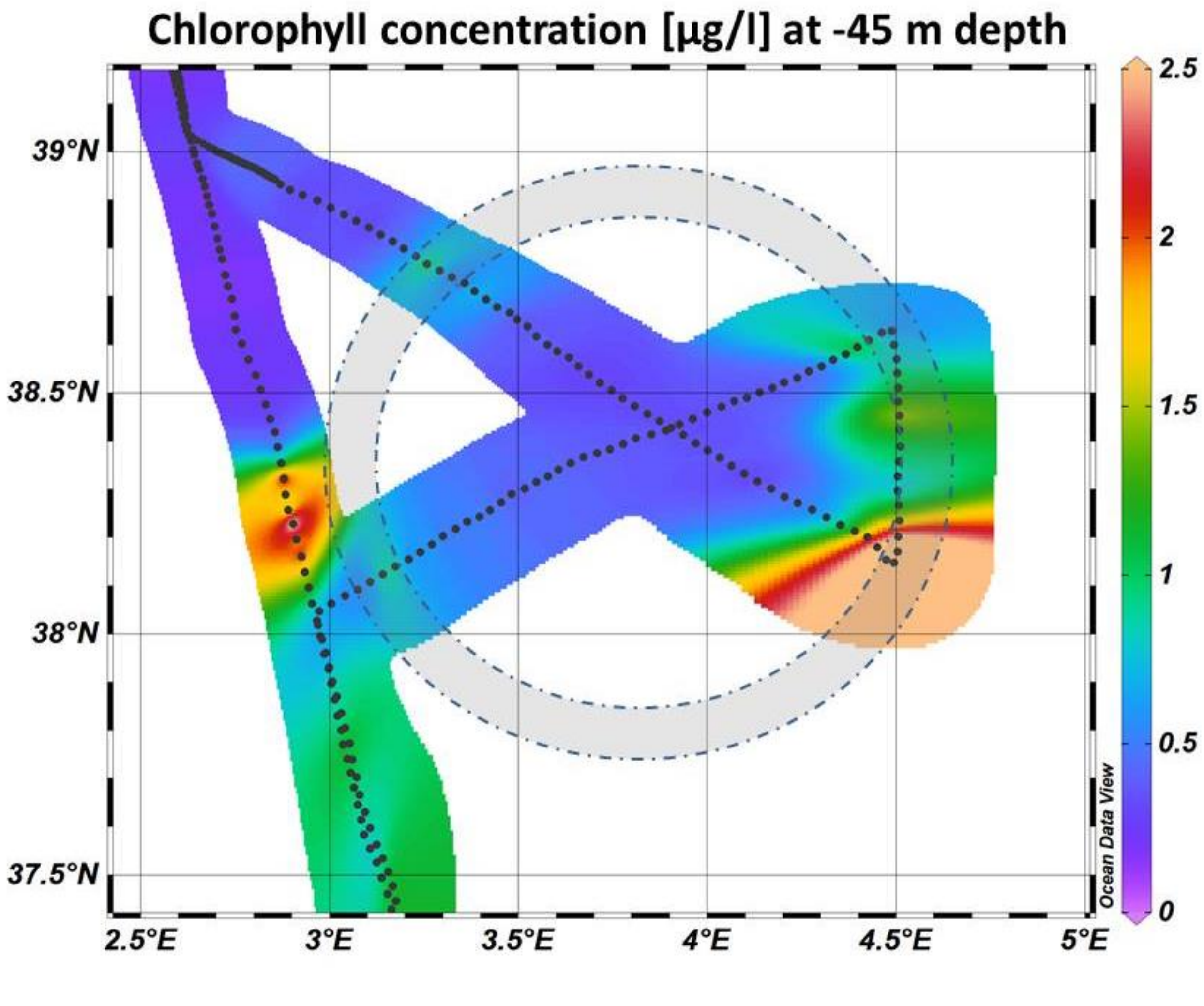

Figures 9: Chlorophyll concentration (µg/l) map at 45 m depth from glider casts (black dots). Grey area identifies the eddy boundary area derived from the estimated radius.

3.4 GEOSTROPHIC AND AGEOSTROPHIC VELOCITIES

Temperature and salinity data collected by the glider have been used to calculate geostrophic velocities (GEOVEL) along three sections in the eddy area (L1, L2 and L3 in Figures 10). As previously described, GEOVEL was referred to 850 dbar, considered as the deepest common depth of all the profiles and according to previous studies in the area (Millot, 2005).

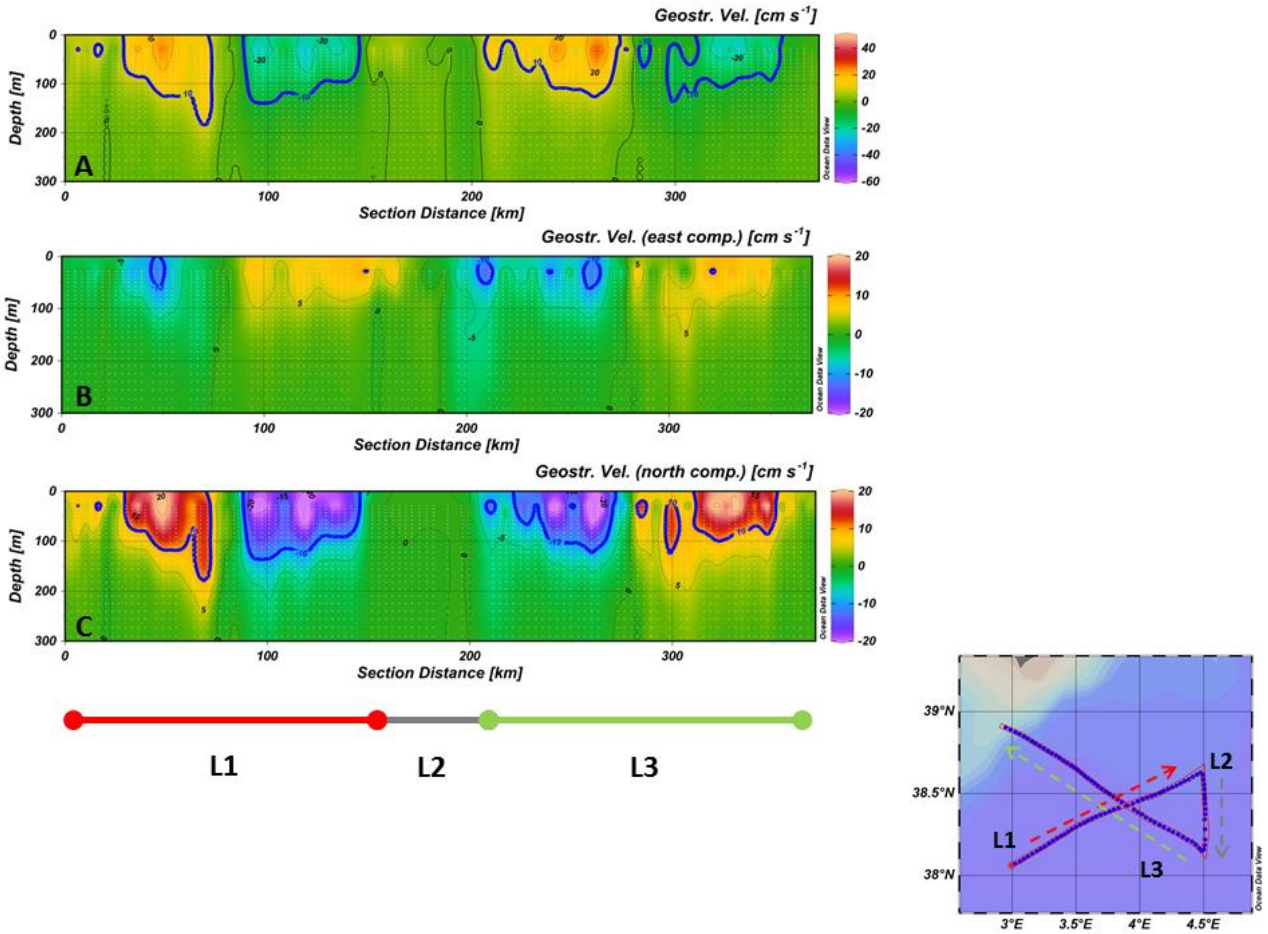

Figures 10: Geostrophic velocity (relative to 850 dbar) calculated from glider CTD data from surface to 300 m depth. Current speed across sections (a), zonal (b) and meridional (c) components are shown. White dots indicate intermediate positions between consecutive glider casts. Sampling transects are indicated in map and along the x-axis of sections.

The data clearly confirm the existence of the anticyclonic circulation in the first 300 m depth associated with the eddy, with higher values confined to the first 100 m. Intense GEOVEL values are found in correspondence with the eddy border, where temperature and salinity variations, previously described, imply a change in the density field. Over depth, GEOVEL values rapidly decrease after the eddy layer, without any significant pattern amongst the sections.

During L1 GEOVEL reach their maximum value (43 cm/s) at about 50 km along the section (Figure 10 a). This maximum is linked to large values calculated for the meridional component of the geostrophic currents that are here directed northwest. After crossing the central eddy area along L1, the geostrophic current is mainly directed southsast, with current speed of about 20 cm/s and a local maximum of 35 cm/s (distance 116 km).

Along the southern part of the L3 transect, geostrophic currents are directed SW and current speeds up to 40 cm/s are found (section distance ~260 km), once again in correspondence with very intense values calculated for the meridional component of the current.

The second part of the L3 section is characterized by GEOVEL directed in the northeast direction with a maximum value of 30 cm/s (section distance 331 km).

All the described maxima are located at about 50 m depth along both transects, at variable distances from the center of the eddy.

The maximum depth reached by the peculiar circulation associated with the eddy structure can be defined on the basis of deepening of velocity isolines. Along L1, the 10 cm/s isoline (absolute value) can reach down to 200 m depth, with the deepest values near the eddy center, while along the SE to NW (L3) section, the same isoline reaches about 150 m depth. This difference could be linked to the 10 day delay between the two transects, and possible evolution of the eddy, becoming shallower in depth.

Figure 11a shows dynamic height at 45 m depth calculated on the regular 5 km grid through Optimal Statistical Interpolation scheme from glider in situ data. Maximum differences of about 10 cm are found between the center and the edge of the eddy. The signature of the anticyclonic eddy is clearly visible in the associated geostrophic velocity field that reaches values of about 30 cm/s. In order to better define the spatial pattern of the anticyclonic eddy, relative geostrophic vorticity has been computed (magnitude of about $\pm 1\text{x}10^{-5}$ s^{-1}). Negative values are found in the center of the domain in correspondence with the large anticyclonic structure while the northeast and northwest of the domain are dominated by positive relative vorticity (Figure 11b).

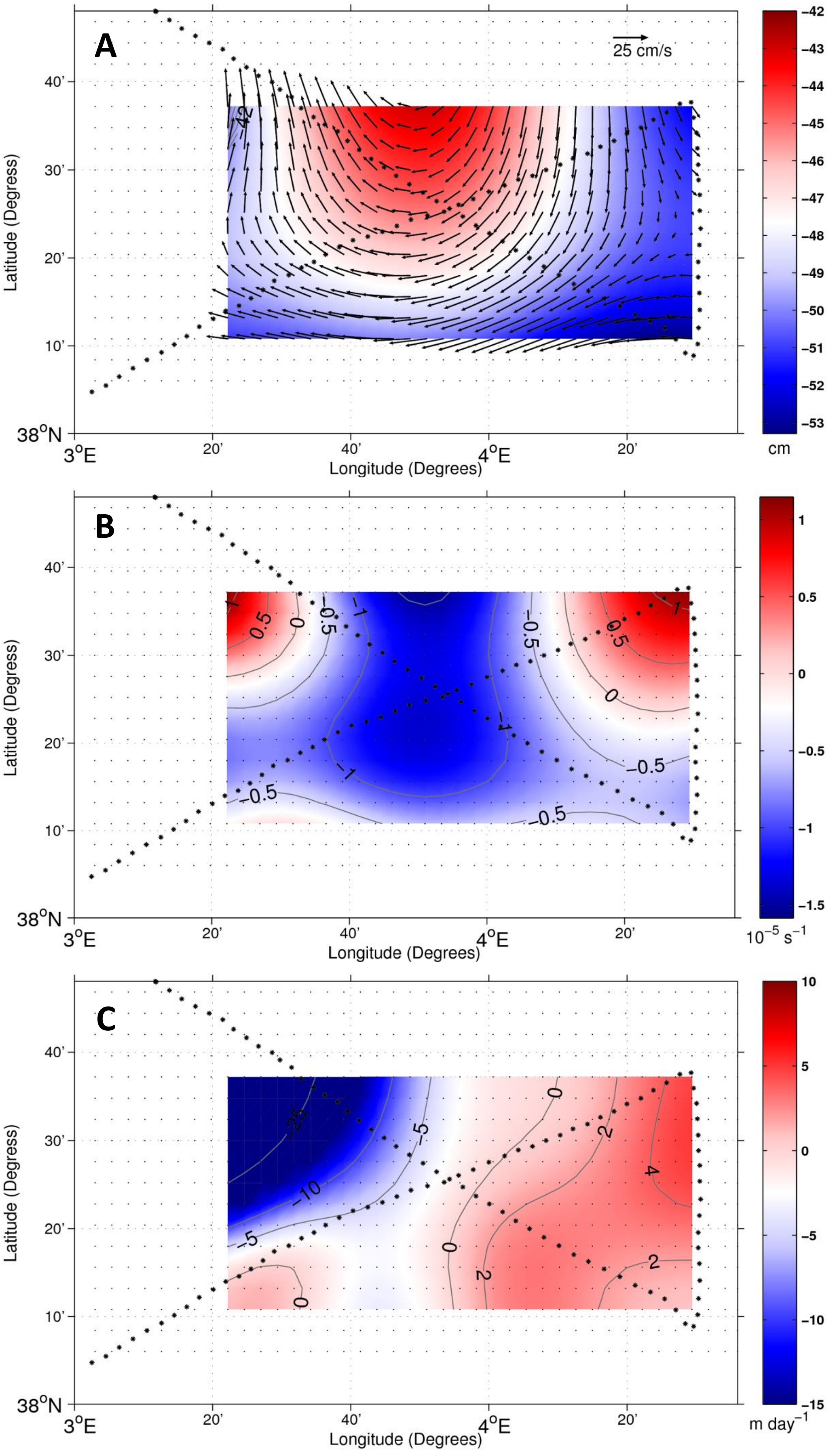

Figures 11: Dynamic height at 45 m depth and associated geostrophic velocities (a), relative geostrophic vorticity (b) and quasi geostrophic vertical velocity (c) calculated on a regular 5 km grid from the Optimal Statistical Interpolation scheme.

Regarding the quasi-geostrophic vertical velocity (QG-w, Figure 11c), values of upward motion (positive) of about +5 m/day have been diagnosed in the eastern part of the domain and downward motion (negative) in the northwestern part (values up to -25 m/day). This pattern in QG-w could explain the general asymmetry observed in the Chl-a field (higher values in the east than in the west). It should be noted that the domain considered to resolve the Omega equation is larger than the dimension of the QG-w field shown in figure 11c, such that the effects of the lateral boundary conditions are not critical. However, negative values are likely overestimated due to the lack of observations in the western part of the domain (in the east, the L2 north-south section is available to close the radial section). Statistical error analysis (not shown) reveals that observed variables and those linearly related to them can be estimated with a relative error (rms error relative to the standard deviation of the field) smaller than 10-15% in the inner domain. For variables not linearly related to observed variables (e.g., quasi-geostrophic vertical velocity) the error can reach values up to 30% (Gomis and Pedder, 2005).

Station distribution and differences in the data used may also account for differences between the sea level anomaly maps and SSH from glider and AVISO data.

Vertical motion diagnosed in this study is coherent in terms of spatial pattern and magnitude, with the horizontal gradients of the geostrophic vertical vorticity (not shown). Therefore, a water parcel under the effect of moderate vertical motion is simultaneously affected by the horizontal velocity, which can result in small vertical displacement of that water parcel and decorrelate the regions of Chl-a maxima.

3.5 SEA SURFACE HEIGHT, TEMPERATURE AND CHLOROPHYLL CONCENTRATION FROM SATELLITE DATA

AVISO SLA maps have been used to identify the position of the mesoscale structure and to modify the track of the glider in order to intercept and sample the eddy along its main axes. Moreover SLA maps allow us to study additional eddy parameters like the mean radius, amplitude, or translation speed. Maps of SLA and associated geostrophic velocity anomalies over the entire Algerian Basin from early June 2014 to the end of October 2014, when operations at sea ended, have been used to track the eddy path since its spawning on early June. The eddy sampled by the glider has been tracked on the basis of the position occupied by the maximum of sea level anomaly in consecutive altimetry snapshots.

The eddy was generated by splitting from another positive sea level anomaly located at 6°E/37.5°N (Figure 12). This first anomaly corresponds to the Eastern Algerian Gyre (EAG) already described by Testor et al. (2005). This gyre has an almost stable position during our investigation period, only moving seaward after one month and approaching the Algerian coast once again at the end of October.

On the other hand, the studied eddy rapidly moves north-west toward the island of Mallorca and reaches its final position where it is located until the end of the glider mission, without further significant interaction with other low/high SLA structures. Its main track derived from the comparison of consecutive SLA maps (blue line in figure 12) since spawning (blue dot) is represented in figure 12 together with SLA map at the end of glider mission, when the eddy center (blue star) is still visible.

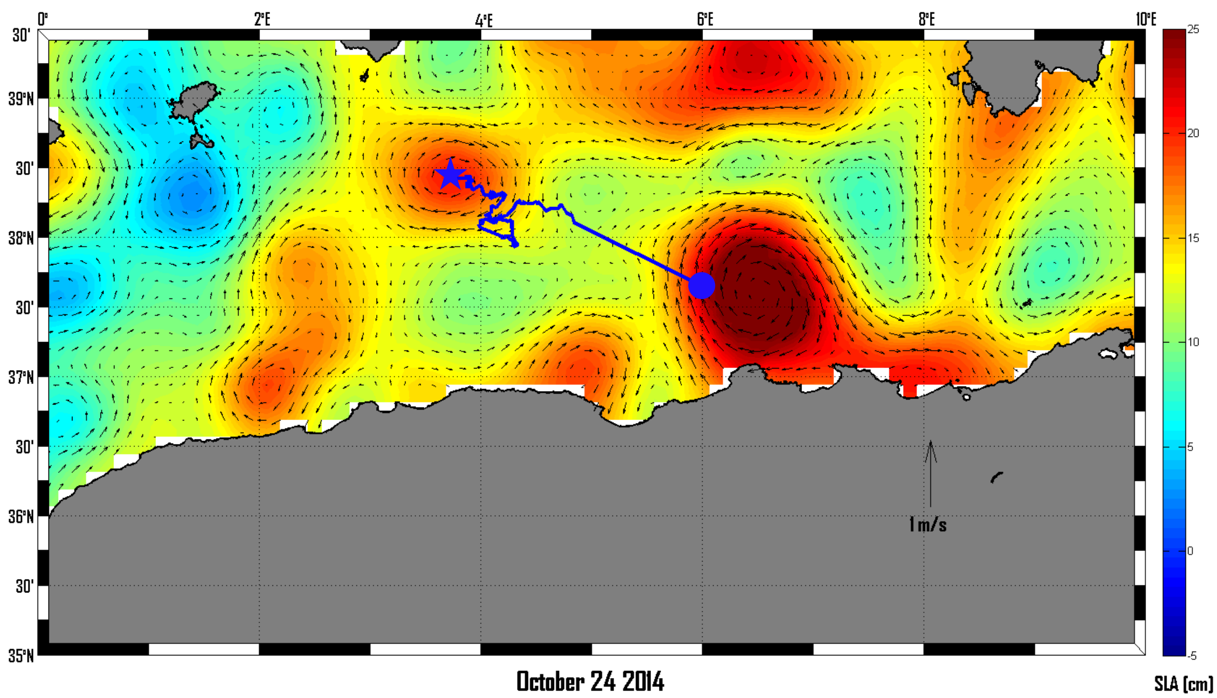

Figure 12: Sea level anomaly map (color scale) and associated geostrophic velocity anomalies (black arrows) from AVISO data on 24 October 2014. Blue line shows the eddy track from its birth in early June to October 2014.

The persistence of the EAG just west of the Sardinia channel and the northwestern direction followed by the sampled eddy is in agreement with the expected route for the AEs. In fact, as described by Millot and Taupier-Letage (2005), eddies that detach from the AC cannot cross the

Sardinia channel due to their size and vertical extent and are expected to propagate along the deeper slope. In our case, the eddy sampled by the glider is pinched off by a big positive anomaly blocked before the Sardinia channel, while the eddy itself is able to move westward joining the general cyclonic circulation of the basin.

After spawning the sampled eddy seems to have had no further interaction with the AC system. It seems instead to have probably been in contact (i.e., end of June and early September, SLA maps not shown) with water masses from the northeastern part of the basin that may have contributed, together with evaporation processes, to the enrichment in salt of the eddy surface waters.

Eddy parameters such as amplitude and radius are not constant during the observed period. Amplitude, estimated as the SLA value in the center of the eddy, reaches a maximum of 21.54 cm above the mean sea surface, with a mean amplitude during the studied period of 15.7 cm. Eddy radius during the glider cruise has been estimated on the basis of both in situ and remote sensed data.

A mean radius of 56.8 and 65.5 km was estimated along the glider transects using surface salinity and maximum sub-surface geostrophic velocity values respectively. Similar results (62.5 km) were found considering altimetry data along the glider track.

Moreover, in order to obtain more robust results on the eddy location and limits, an objective method has been considered through application of a new eddy tracker developed by Mason et al. (2014). Results estimated during the glider cruise period through this algorithm agree well with estimates obtained in this work (eddy radius, 49.8 km; position of eddy center 38.341°N/3.833°E).

The translation speed of the eddy has been derived on the basis of the eddy center position in consecutive satellite altimetry images. Two different tests reveal a mean speed of the eddy of about 4 km/day along its track from its origin to the area south of Mallorca where it stays until the end of the glider cruise. This speed value is in good agreement with the previous literature, describing a speed of a few km per day on atypical along-slope route from the AC area toward Sardinia followed by most such eddies (Ruiz et al., 2002; Millot and Taupier-Letage, 2005). Geostrophic current anomalies show the expected anticyclonic circulation associated with the positive sea level anomaly of the eddy and the spatial pattern is in good agreement with geostrophic velocities retrieved by glider thermohaline data.

In order to better describe the eddy related dynamics in SST and Chl-a features, MODIS level-2 daily maps at 1 km resolution have been acquired and analyzed. Due to persistent cloud cover over the studied area, the attention has been focused on the 26 September 2014 maps (Figure 13a, b). The SST pattern shows the presence of a filament of relatively colder water (≈25 °C) probably of AC origin that wraps and isolates a warmer eddy (≈26 °C) southeast of Mallorca (Figure 13a). A similar filament is present also on the western boundary of the large anticyclonic anomaly located at 6.0°E and 37.5°N representing a deviation of the AC caused by the presence of the mesoscale structure (EAG) from which the sampled Algerian eddy originates. Due to this interaction between the AC and this persistent mesoscale structure, the AC seems to flow perpendicularly to the coast during the monitoring period in agreement with previous observations (Millot et al. 1997; Taupier-Letage and Millot 1988; Ruiz et al. 2002).

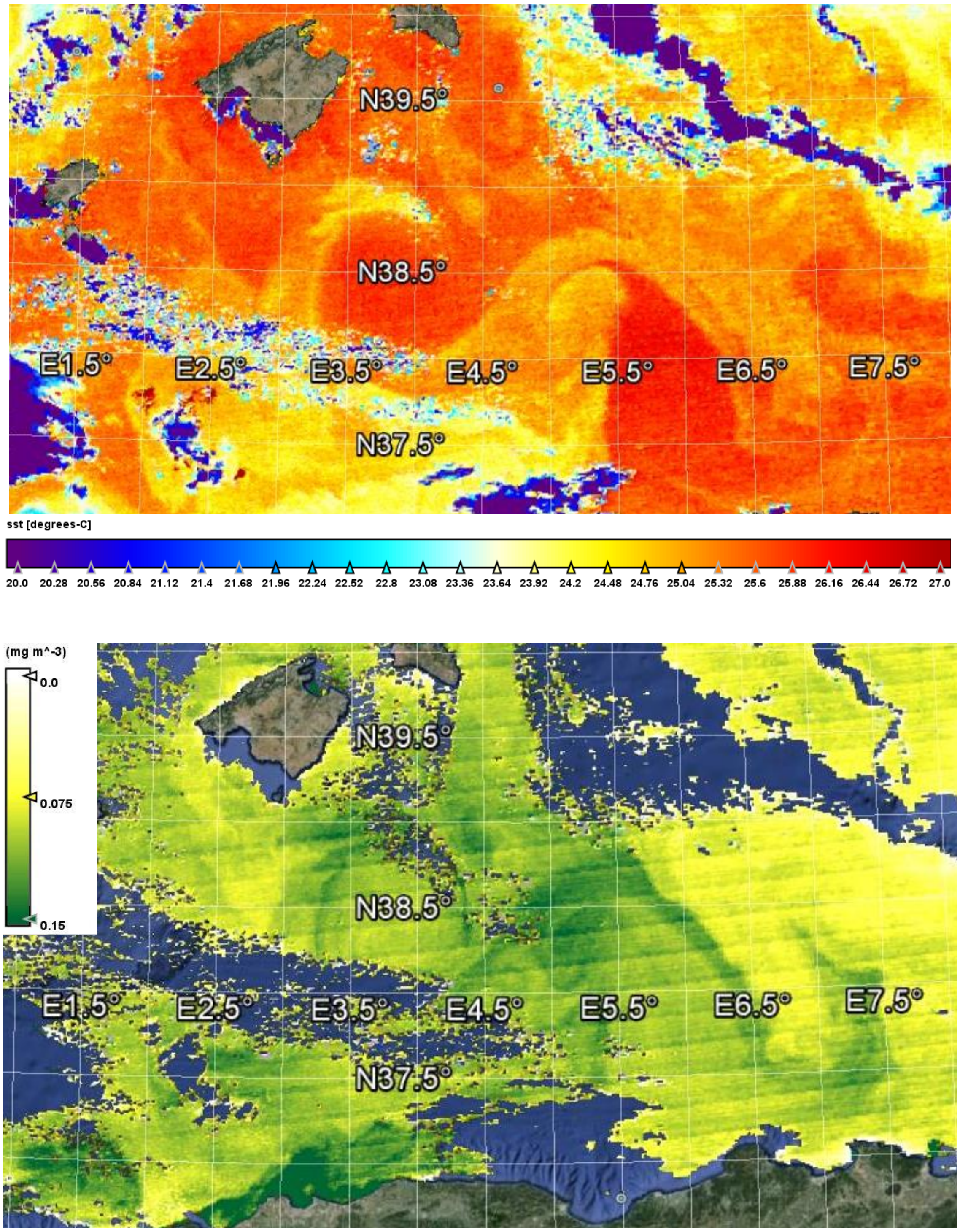

Figure 13: Sea surface temperature at night (a) and chlorophyll concentration (b) at 1 km resolution from MODIS L2 data on the 26 September 2014. Both maps show the presence of the investigated mesoscale eddy.

Even if most of the Chl-a maps are strongly affected by cloud cover during the glider mission, it is possible to identify several interesting features in the 26 September snapshot. The presence of the colder filament described in the SST maps seems to have a remarkable effect on the surface Chl-a pattern. In fact, the highest productivity values are found along this filament (Figure 13b). This is true also in correspondence with the eddy's border where satellite maps show higher Chl-a values (≈0.15 mg/m^3) with respect to the eddy center (≈0.03 mg/m^3). These values totally agree with in situ surface measurements (5 m depth) recorded by the glider across the eddy and along its borders where high sub-surface Chl-a concentrations are observed (Figures 6, 7 and 8). Moreover, satellite maps show the presence of higher Chl-a concentration along the southeastern side of the eddy, thus confirming the high productivity values observed by the glider at 45 m depth in that region (Figure 9).

In order to bypass cloud cover limitations, MODIS level-3 3-days average SST and Chl-a maps at 4 km resolution relative to the period of activities at sea (not shown) were acquired. SST and Chl-a patterns have been confirmed as well as the details on origin, track, evolution and radius of our eddy that are better described on the basis of altimetry data.

4 CONCLUSIONS AND DISCUSSIONS

Combining the use of AUV observations and remote sensing data, the structure of a mesoscale eddy in the Algerian basin has been analyzed. Multi-platform data show the evolution and characteristics of the eddy detaching from the Algerian Current and highlight the effect of the associated dynamics on biochemistry and on chlorophyll concentration patterns. The eddy was identified in the Algerian Basin and then monitored through a dedicated Slocum deep glider mission (September-October 2014).

Satellite data have allowed us to describe the eddy track from its origin in the Algerian Current at 6°E and 37.5°N, the typical position of the persistent EAG, to its last recorded position south of Mallorca. The eddy was characterized by a mean diameter of 112/130 km and a mean elevation in the center of the eddy of 15.7 cm with a clear footprint down to 300 m in salinity, temperature and density, even if no change in mixed layer depth is associated with its presence.

Thermohaline characteristics of water masses trapped in the eddy coincide with temperature and salinity data observed in the southern part of the basin, thus confirming the origin of the eddy from the AC as also shown by satellite data. The surface layer of the eddy is occupied by AW at different modification levels, while intermediate layers are characterized by the presence of LIW. The anticyclonic circulation associated with the eddy is evident in geostrophic velocities calculated from glider CTD data across transects, on a regular 5 km grid obtained through Optimal Interpolation Statistic scheme and in geostrophic velocities derived from satellite altimetry data.

Multiparameter sections and current patterns, have allowed us to characterize the hydrographic and biochemical structure associated with the eddy presence. Shoaling of isolines on the eddy border is evident for all the physical parameters, as well as for Chl-a. Coincidence of maxima chlorophyll values with the eddy border and estimated vertical quasi-geostrophic velocities suggests that positive (upward) velocities on the eastern eddy border may upwell intermediate water and associated nutrients to the photic layer, hence triggering enhanced productivity. Furthermore, as the Chl-a pattern shows some asymmetry on the horizontal plane with the highest values in the southeastern eddy sector, advection effects from the NE sector of the eddy to the SE sector are possible, which may be the source of the high Chl-a values.

This dataset, collected during the ABACUS glider mission supported by JERICO and integrated with satellite information, contributes to an increasing array of observations in the Southern Mediterranean Sea, an area traditionally lacking in situ measurements. Furthermore, it represents the first experiment in this basin using new glider technologies. Finally, it confirms the importance of AEs in the general circulation of the basin and the effect of their presence on the AC path and on biochemical variability.

Moreover, results underline several aspects that may be improved during future ABACUS glider missions focused on the monitoring of mesoscale eddies:

- Spatial resolution of glider observations may be increased to 2 km through the acquisition of data during both upcasts and downcasts. This will allow us to observe small scale structures that may have an effect on the distribution of biochemical parameters as suggested by the observed oxygen concentration patterns.
- Glider tracks across the eddy area and acquisition of data along all the borders of the eddy may be designed in order to improve the results of the applied interpolation procedures and the general description of eddy properties, structure and shape.
- Variations in geostrophic velocities and physical properties observed between the first and second transect also highlight the importance of a synoptic description of the eddy. This may be achieved through the use of a faster platform (i.e. SeaSoar and/or research vessels) or through the realization of a cost effective monitoring by two or more gliders eventually operating at reduced depths.

On the other hand, future studies of the Algerian Basin should also focus on the temporal variability along the Mallorca-Algeria repeat line and on the comparison between high-resolution glider and altimetry data.

ACKNOWLEDGMENTS

The authors are grateful to Marc Torner Tomas and the SOCIB glider Facility, Data Centre and Engineering and Technology Deployment staff for their efficient cooperation. We also thank Dr. Evan Mason for providing results from his eddy tracker and for his precious comments.

The ABACUS mission was funded by Joint European Research Infrastructure network for Coastal Observatories (JERICO) Trans National Access (TNA) third call. Additional EU funding (PERSEUS Grant agreement no: 287600) is acknowledged.

The activities described in this paper have been developed in the framework of the Italian Flagship Project RITMARE.

The altimeter products were produced by Ssalto/Duacs and distributed by Aviso, with support from Cnes (http://www.aviso.altimetry.fr/duacs/).

MODIS data have been retrieved through the website http://oceancolor.gsfc.nasa.gov/cms/.

REFERENCES

Ackerman, S.A., Strabala, K., Menzel, W.P., Frey, R.A., Moeller, C.C., Gumley, L.E., Baum, B.A., Shaaf, C., Riggs, G., 1997. Discriminating clear sky from cloud with MODIS algorithm theoretical basis document (MOD35). Eos ATBD web site, 125 pp.

Arnone, R., La Violette, P.E., 1986. Satellite definition of the bio-optical and thermal variation of the coastal eddies associated with the African current, J. Geophys. Res. 91: 2351-2364.

Arnone, R. A., Wiesenburg, D. A. Saunders K. D., 1990. The origin and characteristics of the Algerian Current, J. Geophys. Res. 95, 1587-1598.

Bouffard, J., Pascual, A., Ruiz, S., Faugère, Y., Tintoré, J., 2010. Coastal and mesoscale dynamics characterization using altimetry and gliders: A case study in the Balearic Sea. J. Geophys. Res. 115, C10029.

Brannigan, L., Marshall, D., Naveira-Garabato, A., Nurser, G., 2015. Generation of submesoscale filaments in the mixed layer of mesoscale vortices. Pers. Comm. 26th IUGG General Assembly 2015 Prague (CZE).

Brown, O.B., Minnett, P.J., 1999. MODIS infrared sea surface temperature algorithm, Algorithm Theoretical Basis Document (ATBD) Version 2.0. ATBD-MOD-25.
On-line document available at: http://modis.gsfc.nasa.gov/data/atbd/ocean_atbd.html

Capet, A., Mason, E., Rossi, V., Troupin, C., Faugère, Y., Pujol, I., Pascual, A., 2014. Implications of refined altimetry on estimates of mesoscale activity and eddy-driven offshore transport in the Eastern Boundary Upwelling Systems, GRL, 41 (21) 7602-27610.

Cetinìc, I., Perry, M. J., D'Asaro, E., Briggs, N., Poulton, N., Sieracki, M.E., Lee, C.M., 2015. A simple optical index shows spatial and temporal heterogeneity in phytoplancton community composition during the 2008 North Atlantic Bloom experiment. Biogeosciences, Vol. 64, pp. 431-451.

Cusi,S., Torner, M., Martinez-Ledesma, M., Roque,D., Beltran, J.P., Ruiz, S., Casas, B., Castilla, C., Lizaran, I., Lora, S., Heslop, E., Tintoré, J., 2013. On the setup of an operational autonomous underwater glider facility . Conference paper 5th MARTECH, Girona (Spain); 10/2013

Escudier, R., 2015. Mesoscale eddies in the Western Mediterranean Sea : characterization and understanding from satellite observations and model simulations. PhD Thesis.

Font, J., Millot, C., Salas, J., Julià, A., Chic, O., 1998. The drift of modified Atlantic water from the Alboran Sea to the eastern Mediterranean. Sci. Mar. 62 (3), 211-216.

Font, J., Isern-Fontanet, J., Salas, J.J., 2004. Tracking a big anticyclonic eddy in the Western Mediterranean Sea. Sci. Mar. 68(3), 331-342.

Fuda, J.L., Millot, C., Taupier-Letage, I., Send, U., Bocognano, X., 2000. XBT monitoring of a meridian section across the Western Mediterranean Sea. Deep-Sea Res. 47 (11), 2191-2218.

Fusco, G., Manzella, G. M. R., Cruzado, A., Gacic, M., Gasparini, G. P., Kovacevic, V., Millot, C., Tziavos, C., Velasquez, Z. R., Walne, A., Zervakis, V., and Zodiatis, G., 2003. Variability of mesoscale features in the Mediterranean Sea from XBT data analysis, Ann. Geophys. 21, 21–32.

Gentemann, C. L., Wentz, F. J., 2001. Satellite microwave SST: Accuracy, comparisons to AVHRR and Reynolds SST, and measurement of diurnal thermocline variability, in Proceedings of the IEEE International Geoscience and Remote Sensing Symposium, IGARSS’01, 246-248.

Gomis, D., Ruiz S., Pedder M.A., 2001. Diagnostic analysis of the 3D ageostrophic circulation from a multivariate spatial interpolation of CTD and ADCP data, Deep Sea Res., Part I 48, 269-295.

Gomis, D., Pedder, M., 2005. Errors in dynamical fields inferred from oceanographic cruise data. Part I:The impact of observation errors and the sampling distribution. J. Mar. Syst. 56, 317–333. doi:10.1016/j.jmarsys.2005.02.002.

Kara, A.,B., Rochford P. A., Hurlburt, E., 2000. An optimal definition for ocean mixed layer depth, J. Geophys. Res., Vol. 105, 16,803–16,821.

Iacono, R., Napolitano, E., Marullo, S., Artale, V., Vetrano, A., 2013. Seasonal Variability of the Tyrrhenian Sea Surface Geostrophic Circulation as Assessed by Altimeter Data. J. Phys. Oceanogr. 43, 1710-1732.

Isern-Fontanet, J., Font, J., Garcìa-Ladona, E., Emelianov, M., Taupier-Letage, C., 2004. Spatial structure of anticyclonic eddies in the Algerian basin (Mediterranean Sea) analyzed using the Okubo-Weiss parameter. Deep-Sea Res. II, Vol. 51, pp. 3009-3028.

Lohrenz, S.E., Arnone, R.A., Wiesenburg, D.A., Depalma, I.P., 1988a. Satellite detection of transient enhanced primary production in the Western Mediterranean Sea. Nature 335, 245-247.

Lohrenz, S.E., Arnone, R.A., Wiesenburg, D.A., Depalma, I.P., Johnson, K.S., Gustafson, D., 1988b. Interrelationships among primary production, chlorophyll, and environmental conditions in frontal regions of the Western Mediterranean Sea. Deep-Sea Res. 35, 793-810.

Mason, E., A. Pascual, McWilliams, J. C., 2014: A new sea surface height based code for mesoscale oceanic eddy tracking. J. Atmos. Oceanic Technol., 31 (5), 1181–1188, doi:10.1175/JTECH-D-14-00019.1.

Merckelbach, L., Briggs, R.D., Smeed, D., Griffiths, G., 2008. Current measurements from autonomous underwater gliders. IEEE, 61–67. doi:http://dx.doi.org/10.1109/CCM.2008. 4480845.

Millot, C., 1985. Some features of the Algerian current. J. Geophys. Res. 90, 7169-7176.

Millot, C., 1987. The circulation of the Levantine Intermediate Water in the Algerian Basin. J. Geophys. Res. 92, 8265-8276.

Millot, C., Benzohra, M., Taupier-Letage, I., 1997. Circulation in the Algerian basin inferred from the MEDIPROD-5 current meters data. Deep-Sea Res. 44 (9–10), 1467-1495.

Millot, C., 1999. Circulation in the Western Mediterranean Sea. J. Mar. Sys. 20, 423-442.

Millot, C., 2005. Circulation in the Mediterranean Sea: evidences, debates and unanswered questions, Scientia Marina, Vol 69, No S1 (2005) doi:10.3989/scimar.2005.69s15

Millot, C., Taupier-Letage, I., 2005. Additional evidence of LIW entrainment across the Algerian Basin by mesoscale eddies and not by a permanent westward flow. Progr. in Oceanogr. 66, 231-250.

Millot, C., Candela, J., Fuda, J.L., Tber, Y., 2006. Large warming and salinification of the Mediterranean outflow due to changes in its composition. Deep-Sea Res. I, 53 (2006), pp. 655–666.

Moran, X.A.G., Taupier-Letage, I., Vazquez-Domınguez, E., Ruiz, S., Arın, L., Raimbault, P., Estarda, M., 2001. Physical– biological coupling in the Algerian basin (SW Mediterranean): influence of mesoscale instabilities on the biomass and production of phytoplankton and bacterioplankton. Deep-Sea Res. 48, 405-437.

Morel, A., André, J. M., 1991. Pigment distribution and primary production in the Western Mediterranean as derived and modeled from Coastal Zone Color Scanner observations, J. Geophys. Res., 96, 12685-12698.

Niewiadomska, K., H. Claustre, L. Prieur, d'Ortenzio, F., 2008. Submesoscale physical-biogeochemical coupling across the Ligurian current (northwestern Mediterranean) using a bio-optical glider. Limnology and Oceanography 53:2,210–2,225.

Obaton, D., Millot, C., Chabert d'Hie`res, G., Taupier-Letage, I., 2000. The Algerian current: comparisons between in situ and laboratory measurements. Deep-Sea Res. 47 (11), 2159-2190.

Olita, A., Ribotti, A., Sorgente, R., Fazioli, L., Perilli, A., 2011. SLA - chlorophyll-a variability and covariability in the Algero-Proven¸cal Basin (1997-2007) through combined use of EOF and wavelet analysis of satellite data. Ocean Dynamics 61, 89–102.

Pascual A., Pujol, M.I., Larnicol, G., Le Traon, P.Y., Rio. M.H., 2007. Mesoscale mapping capabilities of multisatellite altimeter missions: First results with real data in the Mediterranean Sea. J. Mar. Syst. 65(1-4), 190-211.

Pascual, A., Vidal-Vijandel, E., Ruiz, S., Somot, S., Papadopoulos, V., 2014. Spatio-temporal variability of the surface circulation in the Western Mediterranean: a comparative study using altimetry and modelling. In: The Mediterranean Sea: Temporal Variability and Spatial Patterns, (eds. G. E. Borzelli, M. Gacic, P. Lionello, P. Malanotte-Rizzoli), Technical Report, AGU monograph, Washington, USA, pp. 5-24.

Pedder, M. A., 1993. Interpolation and filtering of spatial observations using successive corrections and Gaussian filters. Mon. Wea. Rev., 121, 2889-2902.

Perry, M.J., Sackmann, B.S., Eriksen, C.C., Lee, C.M., 2008. Seaglider observations of blooms and subsurface chlorophyll maxima off the Washington coast, USA. Limnology and Oceanography 53:2,169–2,179.

Pinot, J.M., Tintoré, J., Wang, D.P., 1996. A study of the omega equation for diagnosing vertical motions at ocean fronts. J. Mar. Res., 54 (2), 239-259.

Puillat, I., Taupier-Letage, I., Millot, C., 2002. Algerian eddies lifetime can near 3 years. J. Mar. Syst. 31, 245-259.

Pujol, M.I., Larnicol G., 2005. Mediterranean sea eddy kinetic energy variability from 11 years of altimetric data, J. Mar. Syst. 58, 121-142.

Rio, M.H., Mulet S., Picot N., 2014. Beyond GOCE for the ocean circulation estimate: Synergetic use of altimetry, gravimetry, and in situ data provides new insight into geostrophic and Ekman currents, Geophys. Res. Lett., 41.

Robinson, A.R., (Ed.), 1983. Eddies in Marine Science, 609 pp., Springer Verlag, New York.

Robinson, A., Golnaraghi, M., 1994. Ocean Processes in Climate Dynamics: Global and Mediterranean examples, The physical and dynamical oceanography of the Mediterranean Sea. Kluwer Academic Publishing.

Rudnick,D., Cole, S.T., 2011. On sampling the ocean using underwater gliders. J. Geophys. Res., Vol. 116, doi: 10.1029/2010JC006849.

Ruiz, S., Font, J., Emelianov, M., Isern-Fontanet, J., Millot, C., Salas, J., Taupier-Letage I, 2002. Deep structure of an open sea eddy in the Algerian Basin, J. Mar. Sys. 33-34, 179-195.

Ruiz S., Pascual A., Garau B., Pujol I., Tintoré J., 2009. Vertical motion in the upper ocean from glider and altimetry data, Geophys. Res. Lett. 36(14), L14607.

Salas, J., Millot, C., Font, J., García-Ladona, E., 2002. Analysis of mesoscale phenomena in the Algerian Basin observed with drifting buoys and infrared images. Deep-Sea Res. I 49(2), 245-266.

Schlitzer, R., 2015. Ocean Data View, http://odv.awi.de.

SMDT-MED-2014 Rio, M.H., Pascual, A., Poulain, P.M., Menna, M., Barceló, B., Tintoré, J., 2014. Computation of a new Mean Dynamic Topography for the Mediterranean Sea from model outputs, altimeter measurements and oceanographic in-situ data, Ocean Sci. Discuss., 11, 655-692.

Taupier-Letage, I., 1988. Biodynamique du Bassin Algerien: Estimation de la reponse biologique à certaines structures moyenne echelle par teledetection (AVHRR et CZCS) et mesures in situ, Ph.D. thesis, 120 pp., Univ. d'Aix-Marseille II, Marseille, France.

Taupier-Letage, I., Millot, C., 1988. Surface circulation in the Algerian basin during 1984. Oceanol. Acta sp. 9, 119-131.

Taupier-Letage, I., Puillat, I., Raimbault, P., Millot, C., 2003. Biological response to mesoscale eddies in the Algerian Basin. J. Geophys. Res. 108(C8), 3245-3267.

Testor, P., Send, U., Gascard, J.C., Millot, C., Taupier-Letage, I., Beranger K., 2005. The mean circulation of the southwestern Mediterranean Sea: Algerian Gyres, J. Geophys. Res. 110, C11017.

Tintoré, J., Vizoso, G., Casas, B, Heslop, E., Pascual, A., Orfila, A., Ruiz, S., Martínez-Ledesma, M., Torner, M., Cusí, S., Diedrich, A., Balaguer, P., Gómez-Pujol, L., Álvarez-Ellacuria, A., Gómara, S., Sebastian, K., Lora, S., Beltrán, J.P., Renault, L., Juzà, M., Álvarez, D., March, D., Garau, B., Castilla, C., Cañellas, T., Roque, D., Lizarán, I., Pitarch, S., Carrasco, M.A., Lana, A., Mason, E., Escudier, R., Conti, D., Sayol, J.M., Barceló, B., Alemany, F., Reglero, P., Massuti, E., Vélez-Belchí, P., Ruiz, J., Oguz, T., Gómez, M., Álvarez, E., Ansorena, L., Manriquez, M., 2013. SOCIB: The Balearic Islands Coastal Ocean Observing and Forecasting System Responding to Science, Technology and Society Needs, Marine Tech. Soc. J., 47, 101-117.

Vidal-Vijande, E., Pascual, A., Barnier, B., Molines, J.M., Tintoré J., 2011. Analysis of a 44-year hindcast for the Mediterranean sea: comparison with altimetry and in situ observations. Sci. Mar. 75(1), 71-86.

FIGURE AND TABLE CAPTIONS

Figure 1: Sea level anomaly map (color scale) and associated geostrophic velocity anomalies (black arrows) from AVISO data on 26 September 2014. Blue line shows the glider track from 15 September to 20 October 2014.

Figure 2: Slocum glider navigation and sampling scheme. During each downcast (red arrow) CTD and oxygen sensors (cyan line) sampled the water column from surface to 975 m, while optical parameters (green line) have been sampled down to 300 m with variable resolution (details in table 1). No data were acquired during upcasts (black arrows).

Figure 3: Potential temperature/salinity diagram (θ/S) for the entire glider mission. Blue and green circles identify data from the southern and northern sectors of the track respectively. Data associated with the eddy area are represented by red dots.

Figures 4: Sections from surface to 800 m depth of potential temperature θ (a), salinity (b) and potential density anomaly σ_0 (c) along the SW/NE axis of the eddy. The first 150 m of the water column for θ (d), salinity (e) and σ0 (f) are also shown.

Figures 5: Sections from surface to 800 m depth of potential temperature θ (a), salinity (b) and potential density anomaly σ_0 (c) along the SE/NW axis of the eddy. The first 150 m of the water column for θ (d), salinity (e) and σ0 (f) are also shown.

Figures 6: Sections from surface to 150 m depth of turbidity (a) and chlorophyll concentration (b) along the SW/NE axis of the eddy. Oxygen concentration (c) is shown for the 0-800 m layer.

Figures 7: Sections from surface to 150 m depth of turbidity (a) and chlorophyll concentration (b) along the SE/NW axis of the eddy. Oxygen concentration (c) is shown for the 0-800 m layer.

Figures 8: Sections from 20 m to 100 m depth of chlorophyll concentration (color scale) and potential density anomaly (black isolines) along the SW/NE (a) and SE/NW (b) axes of the eddy.

Figures 9: Chlorophyll concentration (μg/l) map at 45 m depth from glider casts (black dots). Grey area identifies the eddy boundary area derived from the estimated radius.

Figures 10: Geostrophic velocity (relative to 850 dbar) calculated from glider CTD data from surface to 300 m depth. Current speed across sections (a), zonal (b) and meridional (c) components are shown. White dots indicate intermediate positions between consecutive glider casts. Sampling transects are indicated in map and along the x-axis of sections.

Figures 11: Dynamic height at 45 m depth and associated geostrophic velocities (a), relative geostrophic vorticity (b) and quasi geostrophic vertical velocity (c) calculated on a regular 5 km grid from the Optimal Statistical Interpolation scheme.

Figure 12: Sea level anomaly map (color scale) and associated geostrophic velocity anomalies (black arrows) from AVISO data on 24 October 2014. Blue line shows the eddy track from its birth in early June to October 2014.

Figure 13: Sea surface temperature at night (a) and chlorophyll concentration (b) at 1 km resolution from MODIS L2 data on the 26 September 2014. Both maps show the presence of the investigated mesoscale eddy.

Table1: Sampling rate and vertical resolution of glider data.